

Electrically controllable spin filtering in zigzag phosphorene nanoribbon based normal-antiferromagnet-normal junctions

Ruigang Li(李锐岗)1, Jun-Feng Liu(刘军丰), and Jun Wang(汪军)
Citation: Chin. Phys. B, 2024, 33 (**1**): 017304. DOI: 10.1088/1674-1056/acf82a
Journal homepage: http://cpb.iphy.ac.cn; http://iopscience.iop.org/cpb

What follows is a list of articles you may be interested in

Negative magnetoresistance in Dirac semimetal Cd_3As_2 with in-plane magnetic field perpendicular to current

Hao-Nan Cui(崔浩楠), Guang-Yu Zhu(祝光宇), Jian-Kun Wang(王建坤), Jia-Jie Yang(杨佳洁), Wen-Zhuang Zheng(郑文壮), Ben-Chuan Lin(林本川), Zhi-Min Liao(廖志敏), Shuo Wang(王硕), and Da-Peng Yu(俞大鹏)
Chin. Phys. B, 2023, 32 (**7**): 077305. DOI: 10.1088/1674-1056/accd50

Effect of crystallographic orientations on transport properties of methylthiol-terminated permethyloligosilane molecular junction

Ming-Lang Wang(王明郎), Bo-Han Zhang(张博涵), Wen-Fei Zhang(张雯斐), Xin-Yue Tian(田馨月), Guang-Ping Zhang(张广平), and Chuan-Kui Wang(王传奎)
Chin. Phys. B, 2022, 31 (**7**): 077303. DOI: 10.1088/1674-1056/ac4cbf

Quantum transport signatures of non-trivial topological edge states in a ring-shaped Su-Schrieffer-Heeger double-chain system

Cheng-Zhi Ye(叶成芝), Lan-Yun Zhang(张蓝云), and Hai-Bin Xue(薛海斌)
Chin. Phys. B, 2022, 31 (**2**): 027304. DOI: 10.1088/1674-1056/ac34ff

A first-principles study on zigzag phosphorene nanoribbons terminated by transition metal atoms

Shuai Yang(杨帅), Zhiyong Wang(王志勇), Xueqiong Dai(戴学琼), Jianrong Xiao(肖剑荣), and Mengqiu Long(龙孟秋)
Chin. Phys. B, 2021, 30 (**2**): 027305. DOI: 10.1088/1674-1056/abc0e1

Electronic transport properties of Co cluster-decorated graphene

Chao-Yi Cai(蔡超逸), Jian-Hao Chen(陈剑豪)
Chin. Phys. B, 2018, 27 (**6**): 067304. DOI: 10.1088/1674-1056/27/6/067304

Electrically controllable spin filtering in zigzag phosphorene nanoribbon based normal–antiferromagnet–normal junctions

Ruigang Li(李锐岗)[1], Jun-Feng Liu(刘军丰)[1,†], and Jun Wang(汪军)[2,‡]

[1] *Department of Physics, Guangzhou University, Guangzhou* 510006, *China*
[2] *Department of Physics, Southeast University, Nanjing* 210096, *China*

(Received 14 May 2023; revised manuscript received 6 September 2023; accepted manuscript online 9 September 2023)

We investigated the electric controllable spin-filtering effect in a zigzag phosphorene nanoribbon (ZPNR) based normal–antiferromagnet–normal junction. Two ferromagnets are closely coupled to the edges of the nanoribbon and form the edge-to-edge antiferromagnetism. Under an in-plane electric field, the two degenerate edge bands of the edge-to-edge antiferromagnet split into four spin-polarized sub-bands and a 100% spin-polarized current can be easily induced with the maximal conductance $2e^2/h$. The spin polarization changes with the strength of the electric field and the exchange field, and changes sign at opposite electric fields. The spin-polarized current switches from one edge to the other by reversing the direction of the electric field. The edge current can also be controlled spatially by changing the electric potential of the scattering region. The manipulation of edge current is useful in spin-transfer-torque magnetic random-access memory and provides a practical way to develop controllable spintronic devices.

Keywords: zigzag phosphorene, electrically controllable spin filter, quantum transport

PACS: 73.23.–b, 73.23.Ad, 73.43.Cd, 73.63.–b **DOI:** 10.1088/1674-1056/acf82a

1. Introduction

Over the last few decades, spintronics[1–6] has emerged as one of the most promising fields for the development of next-generation electronic devices. At the same time, two-dimensional (2D) materials with long spin relaxation time, including graphene,[7,8] borophene[9,10] and phosphorene,[11–14] have been successfully isolated and now serve as reliable platforms upon which to devise spintronic devices. Nowadays, 2D material-based spintronic devices, such as spin filters[15] and even magnetically enhanced optoelectronics devices,[16] have been achieved.

In addition to a long spin relaxation time/length, high spin injection efficiency is also essential when devising spintronic devices. Both of these properties have been found in phosphorene.[17–24] According to Ref. [17], the spin-relaxation length of phosphorene exceeds 6 μm at room temperature. Farooq *et al.*[18] found that charge doping can induce edge magnetism in armchair phosphorene nanoribbons and an edge-to-edge antiferromagnetic ground state was found in oxygen-passivated tilted phosphorene nanoribbons.[19] Similar to zigzag graphene nanoribbons,[20] edge magnetism in zigzag phosphorene nanoribbons (ZPNRs) was also reported.[21] A study[22] pointed out that edge magnetism exists even though the lattice is not relaxed. Because the edge states determine the electronic properties of ZPNRs, edge ferromagnetism is helpful when devising ZPNR-based spintronic devices.[23] Even though the edge magnetism in ZPNRs vanishes when the dangling bonds at the zigzag edges are removed or the width of the ribbon is bigger than 3 nm (seven unit cells),[21] it can be re-induced by depositing two EuO stripes at the edges, with the large exchange energy 184 meV.[24]

Spin-polarized current and its effective manipulation are essential for spintronic devices.[25,26] A study has reported that a vertical electric field can be used to manipulate the spin-polarized current in ZPNR-based normal–antiferromagnet–normal (N-AFM-N) junctions.[27] However, the spin-polarized current in anti-zigzag phosphorene antiferromagnet (AFM) junctions cannot be controlled by a vertical electric field, in contrast to the proposal in Ref. [27]. Instead, an in-plane electric field can improve the junction from two aspects: first, the inplane field can effectively control the edge bands of all kinds of ZPNR; second, a strong in-plane electric field can be introduced to the junction more easily than a vertical electric field.

In this study, a ZPNR-based N-AFM-N junction is proposed for generating an in-plane electric field controllable 100% spin-polarized current. In detail, the AFM is an edge-to-edge AFM and it is achieved by depositing two EuO stripes, with antiparallel magnetic moments, at the edges, as shown in Fig. 1(a). Both the band structure of the ZPNR and the spin-polarized current in the ZPNR-based junctions can be effectively modulated by the in-plane electric field. The 100% spin-polarized current can be generated at wide energy intervals when the in-plane electric field is applied and the spin direction of the current can be reversed by reversing the direction of the electric field. We also find that, by properly select-

†Corresponding author. E-mail: phjfliu@gzhu.edu.cn
‡Corresponding author. E-mail: jwang@seu.edu.cn

© 2024 Chinese Physical Society and IOP Publishing Ltd

ing the electric potential of the AFM region, the spin-polarized current can be generated and controlled spatially. The manipulation of the electric field in the nanoribbon's two edges, which can function as separate channels for processing spin-dependent information, is helpful for improving spin-transfer-torque magnetic random-access memories (STT-MRAMs) by influencing the edge current. Furthermore, spin polarization can also be controlled by changing the strength of the electric field and the exchange field, and it is stable when there are disorders and vacancies in the scattering region. Our study provides an easy, practical and promising way to devise spin filters and spin-based transistors.

2. Structure and model

Figure 1(a) is the junction we studied, where the edge-to-edge antiferromagnetism is formed by depositing two EuO stripes at the edges of the scattering region. According to Ref. [24], the phosphorene can be adsorbed on top of the EuO(111) surface and form a stable configuration. Two EuO stripes, with antiparallel magnetic moments to each other, are separated and attached to the different edges of the phosphorene nanoribbon. Furthermore, the electric potential $V_{\rm d}$ and in-plane electric fields can be added to the scattering region. The primitive cell is shown in Fig. 1(b), with the size $a_1 \times a_2$, where $a_1 = 3.27$ Å and $a_2 = 4.43$ Å,[12] respectively. The size of the scattering region is $W \times L = N_W a_1 \times N_L a_2$, where N_W and N_L are the number of unit cells in transverse (y) and longitudinal (x) directions, respectively. The AB sites (red atoms) belong to the bottom layer, while the CD sites (white atoms) to the upper layer, as illustrated in Fig. 1(b).

Without loss of generality, the magnetic moment at edge 1 is pointing along $+z$, while that at edge 2 is along $-z$, as shown in Figs. 1(a) and 1(b), respectively. For spin-up (spin-down) electrons, the extra on-site energy caused by the exchange field increased (decreased) along the y direction linearly. The Hamiltonian of the junction reads

$$
\begin{aligned}
H &= H_\sigma^{\rm b} + \left(H_\sigma^{y} + H_\sigma^{\rm exc}\right)\left[\Theta(x) - \Theta(x-L)\right], \\
H_\sigma^{\rm b} &= \sum_{i,j}\left(t_{ij} c_{i\sigma}^{\dagger} c_{j\sigma} + {\rm h.c.}\right), \\
H_\sigma^{y} &= \sum_{i}\left(\frac{y}{W} - \frac{1}{2}\right) E_y c_{i\sigma}^{\dagger} c_{i\sigma}, \\
H_\sigma^{\rm exc} &= \eta \sum_{i}\left(\frac{y}{W} - \frac{1}{2}\right) M c_{i\sigma}^{\dagger} c_{i\sigma},
\end{aligned}
$$

where $\Theta(x)$ denotes the step function. $H_\sigma^{\rm b}$ is the tight-binding Hamiltonian of the bare phosphorene nanoribbon and $c_{i\sigma}^{\dagger}$ is the creation operator of the site i with spin $\sigma = \uparrow / \downarrow$. t_{ij} represents the hopping integrals and the five hopping integrals are $t_1 = -1.220$ eV, $t_2 = 3.665$ eV, $t_3 = -0.205$ eV, $t_4 = -0.105$ eV and $t_5 = 0.055$ eV,[28] as shown in Fig. 1(b). After checking the edge states and conductance of the junction considering t_3 and t_5, we did not find obvious differences from our presented results. t_3 and t_5 are neglected in this study because these two hopping integrals have a limited impact on the transport property of the ZPNR; H_σ^{y} denotes the effect of the in-plane electric field applied to the phosphorene nanoribbon and $|E_y/2|$ corresponds to the maximal on-site energy induced by the in-plane electric field. $H_\sigma^{\rm exc}$ stands for the exchange energy, $|M/2|$ is the maximal exchange energy; for spin-up (spin-down) electron, $\eta = +1$ (-1). Note that, y in H_σ^{y} and $H_\sigma^{\rm exc}$ denotes the coordinates of sites in the transverse direction, which is shown in Fig. 1(b).

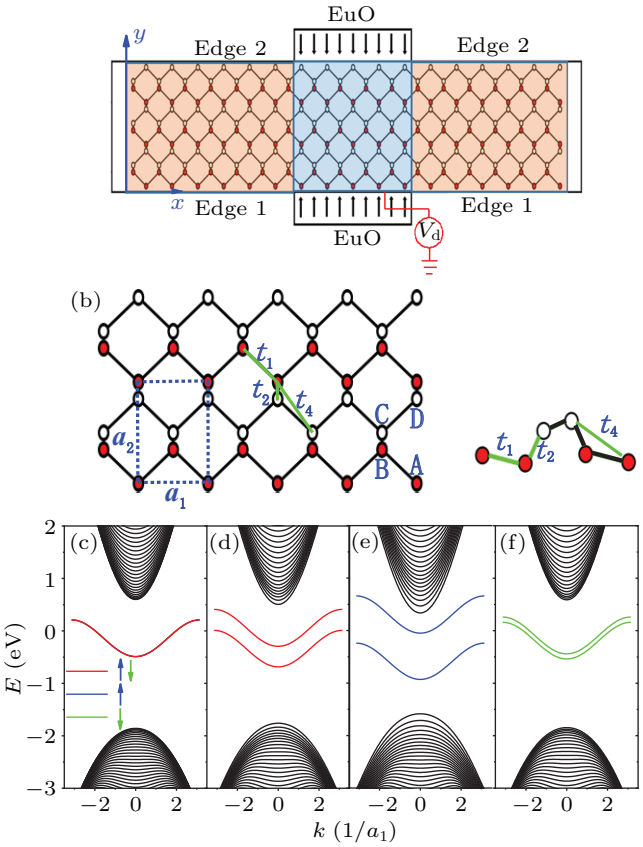


Fig. 1. Schematics of (a) the ZPNR based N-AFM-N junction and (b) the zigzag phosphorene nanoribbon. The band structures of (c) bare ZPNR and (d) edge-to-edge antiferromagnetic ZPNR with $M = 0.4$ eV. Under an in-plane electric field ($E_y = 0.5$ eV), the band structure of the antiferromagnetic ZPNR consists of (e) spin-up bands and (f) spin-down bands. The width of the ZPNR is $W = 40a_2 \approx 17$ nm. All data are given by the Kwant package.[29]

The calculation is done by Kwant,[29] a software for quantum transport calculations. After setting the parameters of the tight-binding model of the junction, the scattering matrix S can be easily obtained. The scattering matrix can be calculated by solving the Schrödinger equations, which makes the calculation speed faster than when using the lattice Green function approach. In this study, the bias drives electrons to flow from the left lead to the right one. The spin-dependent transmission between leads is given as $T_{\rm u(d)}(E_{\rm F}) = \sum_{l,r} \left|S_{l,r}(E_{\rm F})\right|^2_{\rm u(d)}$. The element of scattering matrix $S_{l,r}$ denotes the mode l of the left

lead transmitted to the mode r of the right lead, and u (d) denotes the spin-up (spin-down) electron. According to the Landauer formula, the spin-dependent conductance is proportional to the transmission, given as $G_{\mathrm{u(d)}}(E_{\mathrm{F}}) = e^2 T_{\mathrm{u(d)}}(E_{\mathrm{F}})/h$. The spin polarization is defined as $P = (G_{\mathrm{u}} - G_{\mathrm{d}})/(G_{\mathrm{u}} + G_{\mathrm{d}})$.

3. Results and discussion

Figures 1(c)–1(f) show the band structures of the ZPNR with $N_W = 40$. Four degenerate edge bands lie in the band gap of the bare ZPNR, as shown in Fig. 1(c). When we change the bare ZPNR to an edge-to-edge AFM, the edge bands split into two double-degenerate bands. Each degenerate band consists of one spin-up band and one spin-down band, as shown in Fig. 1(d). In detail, the lower (upper) edge band can be occupied by spin-up (spin-down) electrons localized at edge 1 and spin-down (spin-up) electrons at edge 2. When an in-plane electric field is applied to the nanoribbon along the $+y$ direction, an extra potential difference between edges (E_y) is produced. In this case, the edge bands of spin-up (spin-down) electrons depart from (get close to) each other, which can be found in Figs. 1(e) and 1(f). Based on these special properties, the spin-dependent transport properties of AFM-ZPNR junctions will be significantly different.

In Fig. 2, the variations in spin-dependent conductance and spin-polarization are depicted as a function of the Fermi energy (E_{F}). Without loss of generality, the number of unit cells in the longitudinal (N_L) and transverse (N_W) directions of the scattering region is set to be 50 and 40, respectively, in this study. The in-plane electric field produces an additional on-site potential $E_y/2 = 0.25$ (-0.25) eV on edge 2 (edge 1) of the scattering region. In Fig. 2(a), the spin-dependent conductances are oscillating over a wide energy interval; the oscillation is caused by the quantum interference. G_{d} exists in the energy interval $[-0.3, 0.2]$ eV, with the maximal conductance $2e^2/h$; while G_{u} exists in the energy interval $[-0.5, -0.1]$ eV, with the maximal conductance e^2/h. In Fig. 2(b), the spin polarization shows two obvious platforms in the energy intervals $[-0.5, -0.3]$ eV and $[-0.1, 0.15]$ eV, and the corresponding spin polarizations are 1 and -1, respectively. The oscillation of the polarization in the interval $[-0.3, 0.15]$ eV comes from the mixture of G_{u} and G_{d}. Such phenomena can be understood by the band structures shown in Fig. 1. Note that, compared with Fig. 2(b), the spin polarization in Fig. 2(d) changes sign when the direction of the in-plane field is reversed. The two platforms are separated, which means that such a junction can generate 100% spin-polarized current easily.

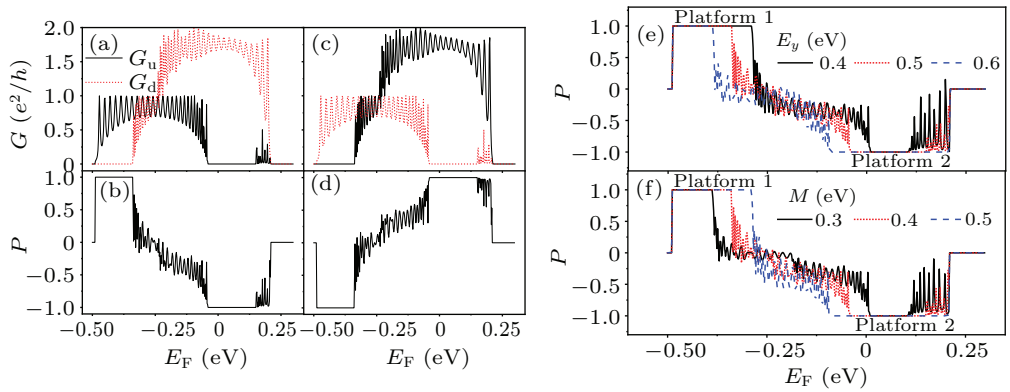


Fig. 2. The spin-dependent conductance and spin polarization of the junction. The parameters are set to be $N_W = 40$, $N_L = 50$, $M = 0.4$ eV and $V_{\mathrm{d}} = 0.2$ eV. (a) (b) $E_y = 0.5$ eV and (c) (d) $E_y = -0.5$ eV. (e) The spin polarization changes with the in-plane electric field E_y, while other parameters are fixed as $N_W = 40$, $N_L = 50$, $M = 0.4$ eV, $V_{\mathrm{d}} = 0.2$ eV. (f) The spin polarization changes with the exchange field M, while other parameters are fixed as $N_W = 40$, $N_L = 50$, $E_y = 0.5$ eV, $V_{\mathrm{d}} = 0.2$ eV.

Besides changing the direction of the electric field, spin polarization can also be effectively tuned by changing the strength of the electric field and the exchange field. In Fig. 2(e), the polarization curve is shifted to lower energy when E_y changes from 0.4 eV to 0.6 eV. The polarization vibration in Fig. 2(e) is evident across a broad energy range when $E_y = 0.4/0.5/0.6$ eV. This phenomenon is attributed to the channels of both spins being built simultaneously in those energy intervals. In Fig. 2(f), when M is increased, platforms 1 and 2 are enlarged and the polarization vibration interval is narrowed. The above properties can be understood by the band structure of the ZPNR.

The spatial distribution of the spin-dependent current is then examined, as shown in Fig. 3(b). The Fermi energy of the junction is set to be $E_{\mathrm{F}} = 0$ eV. From Fig. 3(b), we find that the spin-up electrons are transmitted from the left lead to the right one from edge 1, as the Fermi energy $E_{\mathrm{F}} = E_{\mathrm{F1}}$ lies in the bottom spin-up band, as shown in Fig. 3(a). When the electric potential V_{d} is decreased, the position of the Fermi energy of the scattering region changes from E_{F1} to E_{F2} and electrons will transmit from both edges. In detail, spin-up electrons flow from edge 1 and spin-down electrons from edge 2, with the maximal conductance $G_{\mathrm{u}} = e^2/h$ and $G_{\mathrm{d}} = e^2/h$, respectively. As we further decrease V_{d}, the position of the Fermi energy of the scattering region goes to E_{F3}. The electrons conduct from both edges, with the maximal conductance

$G_{\rm d} = 2e^2/h$. The spin-dependent conductance and spin polarization changes with $V_{\rm d}$ can be found in Fig. 3(c). In brief, this property enables us to control the spin-polarized current spatially by changing the electric potential $V_{\rm d}$ of the scattering region.

The stability of the spin polarization against the disorders and vacancies is also examined. When the disorders are present, an extra potential $V_i^{\rm rom}$ is added to site i of the scattering region, with i running over the scattering region. $V_i^{\rm rom}$ is uniformly distributed in the interval $[-\delta/2,\ \delta/2]$, where δ is the strength of the disorder. The vacancies in the scattering region can be achieved by randomly removing $N_{\rm v}$ atoms from it. The vacancy concentration is defined as $C = N_{\rm v}/(4N_W N_L)$. The results are shown in Fig. 4. In both cases, the spin-dependent conductance is suppressed when δ or C is increased. The maximal $G_{\rm u}$ and $G_{\rm d}$ can reach $0.9e^2/h$ and $1.5e^2/h$, respectively, when $\delta = 0.2|t_1|$ or $C = 2\%$. As we see, the two platforms in the spin-polarization curves remain unchanged when the disorders or vacancies are present.

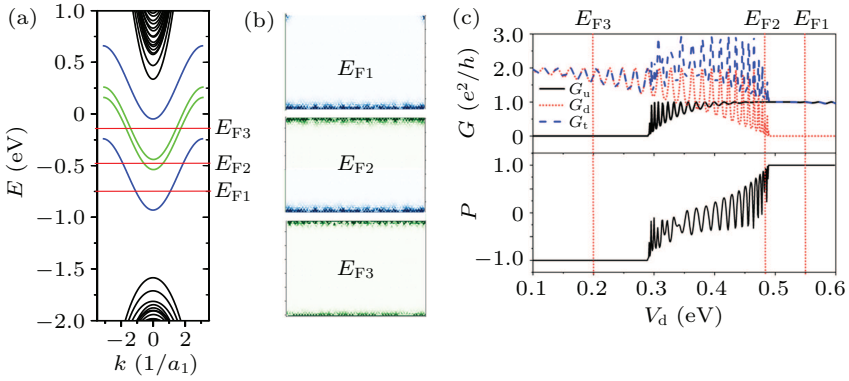


Fig. 3. (a) The band structure of the edge-to-edge AFM ZPNR, with $E_y = 0.5$ eV and $M = 0.4$ eV. (b) The local density of state of electrons when $E = E_{\rm F1/F2/F3}$. (c) The spin-dependent conductance and spin polarization change with the electric potential $V_{\rm d}$ of the scattering region.

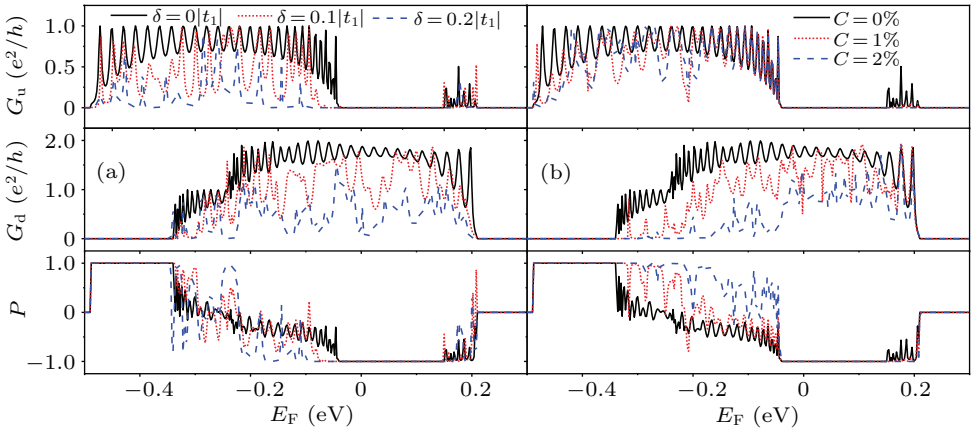


Fig. 4. The spin-dependent conductance and spin polarization of the junction with the presence of (a) disorders with strength $\delta = 0.0|t_1|$, $0.1|t_1|$ and $0.2|t_1|$, or (b) vacancies with concentration $C = 0$, 1% and 2%. The other parameters are set to be $N_W = 40$, $N_L = 50$, $M = 0.4$ eV, $E_y = 0.5$ eV and $V_{\rm d} = 0.2$ eV.

4. Conclusion

In this study, we investigate the spin-filtering effect in a ZPNR-based N-AFM-N junction. The edge-to-edge antiferromagnetism can be achieved by two ferromagnets placed on the edges of the nanoribbon. The two spin-degenerated edge bands of edge-to-edge antiferromagnetic ZPNR separate into four spin-polarized bands when an in-plane electric field is applied to the nanoribbon. A 100% spin-polarized current can be generated at various wide energy intervals in the junction when the in-plane electric field is applied. The spin polarization can be tuned by changing the direction and the strength of the electric field. By changing the electric potential of the scattering region, the edge spin-polarized current can be controlled spatially. In addition to the in-plane electric field, the spin polarization can also be tuned by changing the strength of the exchange field. We also found that the spin polarization is stable when disorders and vacancies are present. Our findings provide a practical way to devise controllable spintronic devices.

Acknowledgements

Project supported by the National Natural Science Foundation of China (Grant Nos. 12174077 and 12174051), the Science Foundation of GuangDong Province (Grant No. 2021A1515012363), and GuangDong Basic and Applied Basic Research Foundation (Grant No. 2022A1515110011).

References

[1] Grichuk E S and Manykin E A 2011 *JETP Lett.* **93** 372
[2] Zhang Q, Chan K S and Lin Z 2011 *Appl. Phys. Lett.* **98** 032106
[3] Bercioux D, Urban D F, Romeo F and Citro R 2012 *Appl. Phys. Lett.* **101** 122405
[4] Michetti P, Recher P and Iannaccone G 2010 *Nano Lett.* **10** 4463
[5] Seneor P, Dlubak B, Martin M B, *et al*. 2012 *MRS Bull.* **37** 1245
[6] Vaklinova K, Hoyer A, Burghard M and Kern K 2016 *Nano Lett.* **16** 2595
[7] Castro Neto A H, Guinea F, Peres N M R, Novoselov K S and Geim A K 2009 *Rev. Mod. Phys.* **81** 1
[8] Geim A K 2009 *Science* **324** 1530
[9] Wang Z Q, Lü T Y, Wang H Q, Feng Y P and Zheng J C 2019 *Front. Phys.* **14** 1
[10] Li W, Kong L, Chen C, Gou J, Sheng S, Zhang W, Li H, Chen L, Cheng P and Wu K 2018 *Sci. Bull.* **63** 282
[11] Li L, Yu Y, Ye G J, Ge Q, Ou X, Wu H, Feng D, Chen X H and Zhang Y 2014 *Nat. Nanotechnol.* **9** 372
[12] Castellanos-Gomez A, *et al*. 2014 *2D Mater.* **1** 025001
[13] Zhang G and Zhang Y W 2017 *Chin. Phys. B* **26** 034401
[14] Yang J and Lu Y 2017 *Chin. Phys. B* **26** 034201
[15] Karpan V M, *et al*. 2007 *Phys. Rev. Lett.* **99** 176602
[16] Fabian J and Žutić I 2008 *Semicond. Sci. Technol.* **23** 114005
[17] Avsar A, *et al*. 2017 *Nat. Phys.* **13** 888
[18] Farooq M U, Hashmi A and Hong J 2015 *ACS Appl. Mater. Interfaces* **7** 14423
[19] Farooq M U, Hashmi A and Hong J 2016 *Sci. Rep.* **6** 1
[20] Jing Y, Zhang X and Zhou Z 2016 *Wires. Comput. Mol. Sci.* **6** 5
[21] Zhu Z, Li C, Yu W, Chang D, Sun Q and Jia Y 2014 *Appl. Phys. Lett.* **105** 113105
[22] Du Y, Liu H, Xu B, Sheng L, Yin J, Duan C G and Wan X 2015 *Sci. Rep.* **5** 8921
[23] Rahman M, Zhou K C, Xia Q L, Nie Y Z and Guo G H 2017 *Phys. Chem. Chem. Phys.* **19** 25319
[24] Chen H, Li B and Yang J 2017 *ACS Appl. Mater. Interfaces* **9** 38999
[25] Nakada K, Fujita M, Dresselhaus G and Dresselhaus M S 1996 *Phys. Rev. B* **54** 17954
[26] Son Y W, Cohen M L and Louie S G 2006 *Nature* **444** 347
[27] Keshtan M A M and Esmaeilzadeh M 2015 *J. Phys. D: Appl. Phys.* **48** 485301
[28] Rudenko A N and Katsnelson M I 2014 *Phys. Rev. B* **89** 1
[29] Groth C W, Wimmer M, Akhmerov A R and Waintal X 2014 *New J. Phys.* **16** 063065